PHYSICAL REVIEW B **93**, 161116(R) (2016)

Active role of nonmagnetic cations in magnetic interactions for double-perovskite $Sr_2BOsO_6(B = Y, In, Sc)$

Sudipta Kanungo,[1,*] Binghai Yan,[1,2,3] Claudia Felser,[1] and Martin Jansen[1,4]
[1]*Max-Planck-Institut für Chemische Physik fester Stoffe, 01187 Dresden, Germany*
[2]*School of Physical Science and Technology, Shanghai Tech University, Shanghai 200031, China*
[3]*Max-Planck-Institut für Physik komplexer Systeme, 01187 Dresden, Germany*
[4]*Max-Planck-Institut für Festkörperforschung, 70569 Stuttgart, Germany*
(Received 9 October 2015; revised manuscript received 28 March 2016; published 29 April 2016)

Using first-principles density-functional theory, we have investigated the electronic and magnetic properties of recently synthesized and characterized 5*d* double-perovskites $Sr_2BOsO_6(B = Y, In, Sc)$. The electronic structure calculations show that in all compounds the Os^{5+} ($5d^3$) site is the only magnetically active one, whereas Y^{3+}, In^{3+}, and Sc^{3+} remain in nonmagnetic states with Sc/Y and In featuring d^0 and d^{10} electronic configurations, respectively. Our studies reveal the important role of closed-shell (d^{10}) versus open-shell (d^0) electronic configurations of the nonmagnetic sites in determining the overall magnetic exchange interactions. Although the magnetic Os^{5+} ($5d^3$) site is the same in all compounds, the magnetic superexchange interactions mediated by nonmagnetic Y/In/Sc species are strongest for Sr_2ScOsO_6, weakest for Sr_2InOsO_6, and intermediate in the case of the Y (d^0) due to different energy overlaps between Os-5*d* and Y/In/Sc-*d* states. This explains the experimentally observed substantial differences in the magnetic transition temperatures of these materials, despite an identical magnetic site and underlying magnetic ground state. Furthermore, short-range Os-Os exchange interactions are more prominent than long-range Os-Os interactions in these compounds, which contrasts with the behavior of other 3*d*-5*d* double perovskites.

DOI: 10.1103/PhysRevB.93.161116

Introduction. Double-perovskite oxides with the general formula $A_2BB'O_6$ are extensively studied and have attracted enormous attention from material science communities over decades owing to their diverse physical properties, such as colossal magnetoresistance (e.g., Sr_2FeMoO_6 [1]), multiferroicity (e.g., Ba_2NiMnO_6 [2]), room-temperature magnetodielectric properties (e.g., La_2NiMnO_6 [3]), optical properties (e.g., Sr_2CrReO_6 [4]), high T_N ferrimagnetism (e.g., Sr_2CrOsO_6 [5]), ferromagnetic-insulator (e.g., Ca_2CrSbO_6 [6]), half metallicity (e.g., A_2CrWO_6 [7]), and metallicity (e.g., Sr_2CrReO_6 [8]). The key elements dictating these properties are transition metals with different *d* orbitals in the *B* and *B'* sublattices. Individually the *B* and *B'* sublattices form two fcc lattices. The entire structure is a combination of two interpenetrating fcc lattices, each of which exhibits intrinsic geometric frustration. The wide range of choices for the *B* and *B'* ions provides a great tunability of intra- and intersublattice interactions. The subtle competition between different exchange interactions can lead to exotic magnetic phases, such as antiferromagnetic (AFM) transitions in the 3*d*-5*d* double-perovskites Sr_2CoOsO_6 [9,10] and Sr_2FeOsO_6 [11,12]. Here, the long-range Os-Co/Fe-Os coupling is found to be surprisingly large mediated by the magnetic Co ($3d^7$)/Fe ($3d^5$).

To investigate the general trend of long-range 5*d*-5*d* exchange coupling, it was considered that d^0 and d^{10} configurations at the *B* site represent two extreme cases for nonmagnetic cations. Recently compounds Sr_2ScOsO_6 (SSOO), Sr_2YOsO_6 (SYOO), and Sr_2InOsO_6 (SIOO) with the AFM transition temperatures of $T_N = 92$, 53, and 27 K, respectively, have been synthesized [13,14]. They display a surprisingly large range of magnetic ordering temperatures, which obviously depend on the type of the nonmagnetic *B* cation incorporated [13,14]. To rationalize the causes of such unexpected behavior, we address these observations in the present theoretical Rapid Communication. The effect of electron filling on magnetic properties has been discussed for other materials in the previous literature [15,16].

In this Rapid Communication, we focus on SYOO and SIOO, both of which have a nonmagnetic *B*-4*d* site and a magnetic *B'*-5*d* site [$Os^{5+}(d^3)$], to investigate the effect of the nonmagnetic cations on the Os-Os exchange couplings. For SYOO, the nonmagnetic site Y^{3+} has a $4d^0$ open-shell configuration. In SIOO, In^{3+} has a closed-shell $4d^{10}$ configuration. These ions provide an ideal platform to compare the d^0 and d^{10} cases. In addition, SSOO is similar to SYOO in that the only difference is the presence of the 3*d* Sc^{3+} ion at the nonmagnetic site, which offers an opportunity to explore 4*d* versus 3*d* cases. We have performed electronic structure calculations based on density-functional theory (DFT) and have analyzed the short-range and long-range magnetic exchange interactions of the Os sublattice. Our calculations reveal that the short-range Os-Os interactions are much stronger than the long-range ones, unlike other double perovskites, such as Sr_2CoOsO_6 [9,10] and Sr_2FeOsO_6 [11,12]. We find that the exchange coupling depends strongly on the overlap between the Os-5*d* and the Y/In/Sc-*d* states in same energy window. The hybridization between Os-5*d* and In-4*d* is much smaller in the d^{10} closed-shell case than that in the d^0 open-shell case, which results in the amplitudes of Os-Os coupling being smaller in the In compound than in the Y and Sc compounds. The smaller exchange coupling in the Y compound versus Sc is attributed to a similar origin, wherein the hybridization of the Sc-3*d* states with the Os-5*d* states in the density of states (DOS) is greater than that for Y-4*d*. Thus, we can successfully explain the varied trend in the Néel temperatures observed experimentally.

*sudipta.kanungo@cpfs.mpg.de

TABLE I. Experimental crystal structure data for SYOO, SIOO, and SSOO.

	SYOO	SIOO	SSOO
Volume (Å^3)	274.8	260.8	253.9
Bond lengths (Os-O) (Å)	1.94,1.96,1.99	1.94,1.97,1.95	1.95,1.96,1.96
Bond angles (<O-Os-O)	90.2,90.9,90.5	92.5,92.7,90.9	92.6,90.7,90.8
Bond angles (<B-O-Os)	157.7,156.6,155.2(c)	160.6,153.9,160.5(c)	165.7,166.2,166.3(c)

Crystal structure and computational details. SYOO, SIOO, and SSOO crystallize in a monoclinic structure with space group $P2_1/n$. The theoretically optimized structures are obtained by relaxing the atomic positions of all atoms while keeping the lattice parameters fixed at their experimentally determined low-temperature (2.9-K) values [13]. The structures consist of alternating corners sharing distorted BO_6 ($B = Y$,In,Sc) and OsO_6 octahedra with Sr atoms situated at the void positions between the two types of octahedra. The six metal-oxygen bond lengths of the distorted octahedra are grouped into three different values. Because of the monoclinic distortion, the in-plane and out-of-plane B-O-Os ($B = Y$,In,Sc) chains deviate substantially ($<B$-O-Os $\sim 155^\circ - 160^\circ$) from an ideal 180° value as shown in Table I. The DFT calculations are performed with the plane-wave basis set based on a pseudopotential framework as implemented in the Vienna *ab initio* simulation package [17]. The generalized gradient approximation (GGA) exchange-correlation functional is employed following the Perdew-Burke-Ernzerhof prescription [18] for calculating the electronic structures. Furthermore the effect of the correlation on the electronic structure was investigated by performing additional GGA + U [19,20] calculations. For the plane-wave basis, a 600-eV plane-wave cutoff is applied, and a k-point mesh of $8 \times 8 \times 6$ in the Brillouin zone is used for the self-consistent calculations.

Results and discussions. First we investigate the electronic structure within the GGA prescription and the calculated ferromagnetic (FM) DOS is shown in Fig. 1. The top, middle, and bottom panels represent the SYOO, SIOO, and SSOO DOS, respectively. The Sr states lie far above the Fermi level (E_f) and are not shown in the figure, which is consistent with the nominal Sr^{2+} valence state. Note that the spin-polarized calculations within the GGA without an artificial Coulomb U drive the insulating solution with very small gaps at E_f. For each compound, only the Os states contribute to the E_f along with a substantial portion from the O-2p states, whereas all Y/In/Sc-d states are either completely empty or filled. For SYOO, the Y-4d states are completely empty and lie almost 5 eV above the E_f, confirming the presence of the Y^{3+} state with a $4d^0$ configuration. On the other hand, in SIOO, the In-4d states are almost 10 eV below the E_f (not shown in the figure), consistent with a completely filled In^{3+} $4d^{10}$ shell. The Os-5d states split according to the octahedral environment of the surrounding oxygen atoms with the t_{2g} states being completely filled in the majority spin channel and completely empty in the minority spin channel. The Os-e_g states are completely empty in both channels. The calculated GGA magnetic moments at the Os site are 2.03, 1.99, and 1.97 μ_B for SYOO, SIOO, and SSOO, respectively, and are consistent with the experimentally measured effective magnetic moments [13]. The Y/In/Sc sites remain nonmagnetic with the zero magnetic moment. The magnetic moments at the O sites are also non-negligible [0.115μ_B (SYOO), 0.123μ_B (SIOO), 0.123μ_B (SSOO)] reflecting the strong hybridization between O-2p and Os-5d states. Together with the calculated magnetic moments, these findings suggest that Os is in the $5 + (5d^3)$ valence electronic state with a high spin ($S = 3/2$) configuration. This result implies that, for these compounds, Os is the only magnetically active site in these compounds with combinations of d^0-d^3 (SYOO and SSOO) and d^{10}-d^3 (SIOO) configurations. Thus, an effective spin model can be constructed in terms of only Os-t_{2g} degrees of freedom. To reveal the effect of the Coulomb U on the electronic structure, we performed a systematic analysis of the electronic structure with $U_{\text{eff}}^{\text{Os}} = 1 - 3$ eV [14,21] (shown in the Supplemental Material [22] Fig. 1 and Table I) and found that a systematic increment in the band gap and magnetic moments at the Os

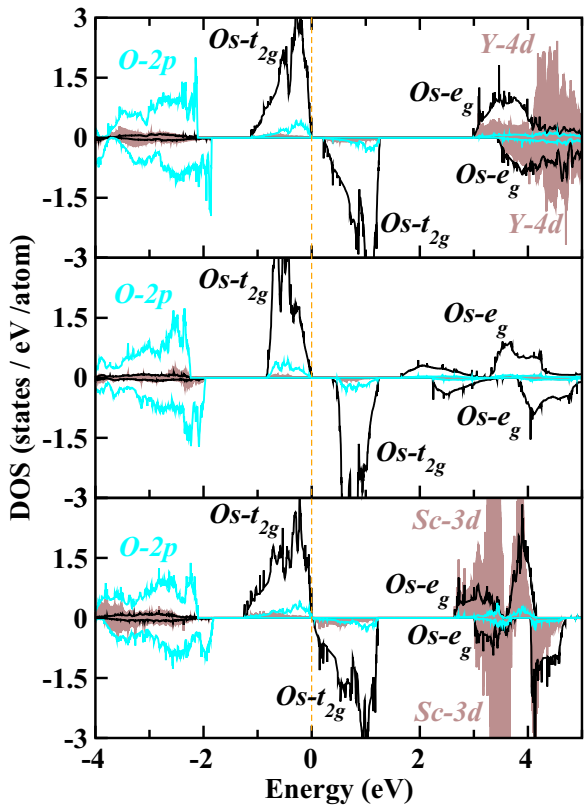

FIG. 1. GGA FM density of states. The top to bottom panels show the DOS for SYOO, SIOO, and SSOO, projected onto the Y-4d-Os-5d, the In-4d-Os-5d and Sc-3d-Os-5d states, respectively, along with the O-2p states. The two channels for each panel represent majority and minority spin channels. The E_f is marked at zero on the energy scale.

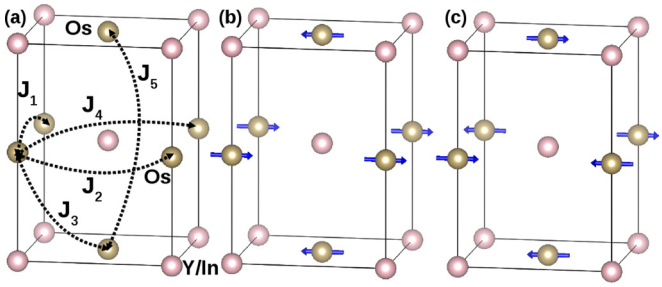

FIG. 2. (a) Magnetic exchange paths connecting different Os sites (brown spheres) in the monoclinic unit cell of Sr_2BOsO_6 ($B = Y$,In, Sc). Sr and O atoms are omitted from the structure for clarity. The five interaction paths between different Os sites are denoted by $J_1 - J_5$. The two lowest magnetic spin structures, (b) experimental spin structure AFM-I and (c) second lowest spin structure AFM-II.

site take place, however no significant changes occurred in the electronic structure and spin states of the compounds in the entire range of U compared to GGA calculations.

Experimental measurements [13] show that the AFM transition temperatures (T_N) of these compounds are very different. To understand the trend in T_N, we decided to calculate the magnetic exchange interactions with DFT-based first-principles calculations. Exchange interactions can be calculated using the Kugel-Khomskii model [23,24], which requires the correct choice of U, the Hund's exchange, and a proper estimate of charge-transfer energies between different orbitals. However, because of the complex exchange paths involving different types of atoms and orbitals, such energies are difficult to estimate. Therefore, we chose a different route using the total energy calculations of various spin configurations and then mapped the DFT total energies onto the corresponding Ising models [25] with the equation $E^{\text{total}} = \Sigma_{ij} J_{ij}\sigma_i\sigma_j$, where J_{ij} is the magnetic exchange interaction between the ith and the jth sites and the $\sigma's$ are the effective spin values corresponding to the respective sites. Although this method suffers from several drawbacks, such as the choice of spin configurations and exchange-correlation functional, the method has helped in successfully estimating qualitative trends in exchange interactions for various types of materials [9–11,26,27]. We used both the GGA and the GGA + U ($U_{\text{eff}}^{\text{Os}} = 1$ and 3 eV [14,21]) to estimate the exchange couplings. To probe the long-range exchange interaction, we created a $2 \times 2 \times 2$ supercell and considered five independent exchange pathways connecting various Os sites as illustrated in Fig. 2(a). The point to be noted is that the GGA and GGA + U calculations gave qualitatively the same trend of exchange interactions for the three compounds with a slight decrease in absolute values due to the inclusion of the U. The GGA results are listed in Table II, whereas the GGA + U results are tabulated in the Supplemental Material [22] and Table III. We also cross-checked the convergence of J values upon varying calculation parameters and found that they depend less than 1% on the calculation parameters, such as plane-wave cutoff, k points, energy convergence, and number of bands.

TABLE III. Magnetic exchange interactions (J_3) calculated with the GGA for SIOO, SYOO, and SSOO in different unit-cell volumes. Diagonal bold entries are the values for each compound within its own structure (from Table I).

	Magnetic exchange interaction (J_3) meV		
	SIOO volume	SYOO volume	SSOO volume
SIOO	**1.47**	1.22	
SYOO	4.38	**3.90**	4.66
SSOO		5.39	**6.47**

Two interesting trends can be identified from the results. First, the short-range Os-Os interactions are much larger than the long-range Os-Os interactions. For example, the Os-O-B-O-Os nearest-neighbor interactions (J_1, J_2, and J_3) are much stronger than the next-nearest-neighbor interactions (J_4 and J_5). This trend is opposite to what we found in previous studies of $3d$-$5d$ double-perovskite Sr_2CoOsO_6 [9,10], Sr_2FeOsO_6 [11], and Sr_2NiIrO_6 [28] where the nearest-neighbor interactions are much weaker than the next-nearest one. The major electronic difference is that, in the present case, Os is the only magnetically active site, whereas for the compounds in the previous studies [9,10,11,28], both B(Fe,Co,Ni) and B'(Os,Ir) were magnetically active.

Because the transition metal at site B is magnetically inactive in the present compounds, the long-range supersuperexchange interaction between two Os sites (Os-O-B-O-Os), connected by a 180° -site-mediated ligand network, becomes weaker than the nearest neighbor direct exchange interactions between two Os sites connected by a 90° ligand network. This is clearly visible in Fig. 3.

Another interesting observation is that the strength of the exchange interactions is stronger for SYOO than for SIOO. For example, the strongest nearest-neighbor interactions (J_1, J_2, and J_3) for SYOO are almost double those of SIOO, whereas the next-nearest-neighbor interactions are an order of magnitude stronger for SYOO than for SIOO. These

TABLE II. Magnetic exchange interactions calculated with GGA for the paths shown in Fig. 2(a). The values of J (meV) for SYOO, SIOO, and SSOO are listed in the table below with (+) and (−) signs indicating AFM and FM interactions, respectively. Exchange interaction values for Sr_2FeOsO_6 are shown for comparison from Ref. [11].

Interaction paths [Os-Os]	Sr_2YOsO_6	Sr_2InOsO_6	Sr_2ScOsO_6	Sr_2FeOsO_6 [11]
J_1 (in-plane short range)	3.02	1.16	5.24	− 0.2
J_2 (in-plane short range)	4.63	2.52	7.42	
J_3 (out-of-plane short range)	3.90	1.47	6.43	3.3
J_4 (in-plane long range)	0.91	0.04	1.66	− 6.8
J_5 (out-of-plane long range)	0.76	0.08	0.42	12.8

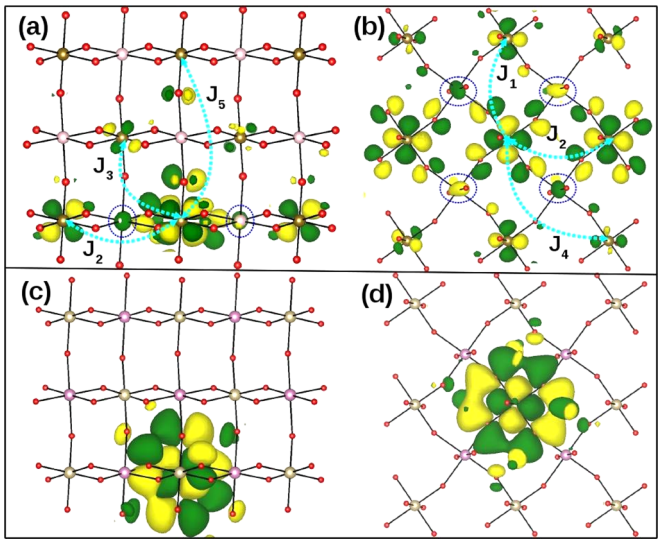

FIG. 3. The Wannier functions of Os-t_{2g}'s for SYOO and SIOO calculated with the GGA prescription are shown in the top [(a) and (b)] and bottom [(c) and (d)] panels, respectively. The central part of the Os Wannier functions comprises Os-5d_{yz} and Os-5d_{xy} characters for (a) and (c) and (b) and (d), respectively. The exchange interactions J_2-J_3-J_5 and J_1-J_2-J_4 are shown in (a) and (b), respectively. The green and yellow colors represent surfaces with isovalues of 0.18 and −0.18, respectively. The red spheres represent O atoms, whereas the other color symbols are the same as those in Fig. 2.

interesting differences can be visualized using a localized Wannier function representation. Figure 3 shows the plots of the effective Wannier-like orbitals located at Os sites corresponding to the Os-Os interactions for both SYOO (top panel) and SIOO (bottom panel). The central parts are composed of Os-d characters, whereas the tails situated at the different sites are shaped according to the integrated out orbitals. The weights at the neighboring tails dictate the strength of interactions between different sites. From Fig. 3(a), we can see that the J_5 (Os-O-Y-O-Os) interaction is very small compared to the J_2 and J_3 interactions because there are large d tails at the connecting Os sites for J_2 and J_3, relative to J_5. Figure 3(b) shows that the in-plane nearest-neighbor J_1 and J_2 (Os-O-Y-O-Os) 90° interactions are similar in strength as indicated by the similar weight of the connecting Os tails, which are much greater than for J_4. It has been suggested in previous studies [9–12,28] that long-range 5d-5d interactions are much stronger than the short-range one due to the extended nature of the 5d wave functions. However, in the present case, even though we have a magnetically active 5d site, the short-range Os-Os interactions (J_1, J_2, and J_3) are much stronger than the long-range ones (J_4, J_5) because of the presence of an interpenetrating nonmagnetic rather than a magnetic B sublattice.

Interestingly, both top panels show significant tails corresponding to the nearest-neighbor interaction at the connecting Os sites, whereas the bottom panel shows almost no tails at the connecting sites. We also observed strong Os-t_{2g} tails at the neighboring Y sites, which are marked by dotted circles in Figs. 3(a) and 3(b); these are completely absent in the case of In as shown in Figs. 3(c) and 3(d). The pictorial representations of the Wannier orbitals clearly indicate the possible role of interpenetrating nonmagnetic Y or In sublattices in determining the overall magnetic interactions.

A point to be noted within the GGA and GGA + U descriptions is that the experimentally observed AFM-I state is energetically higher than AFM-II as shown in Figs. 2(b) and 2(c), respectively, however the inclusion of spin-orbit coupling (SOC) with the GGA drove the experimentally observed AFM-I to a value of ∼1.2 meV/f.u. (where f.u. represents formula units) lower than the AFM-II. These results indicate a strong influence of SOC on the electronic structure as has been suggested in recent studies [29–31] of the $4d^3$ and $5d^3$ t_{2g} systems. We calculated the exchange interactions including SOC for the three compounds and found that the relative strengths of the AFM interactions (J_3) for SYOO (3.67 meV), SIOO (1.46 meV), and SSOO (5.55 meV) remained unchanged upon addition of SOC. Here we want to mention that we restrict ourselves in evaluating only the symmetric part of the exchange interactions ignoring the antisymmetric ($\mathbf{S}_i \times \mathbf{S}_j$) type of exchanges even in the presence of SOC. The antisymmetric exchange will only arise due to canting of spins ($\mathbf{S}_i \times \mathbf{S}_j$), and in the collinear spin configuration, this part vanishes. We neglected this antisymmetric type of exchange because the experimentally observed antiferromagnetic configuration is a collinear AFM where spins are aligned in parallel to the ab plane. Therefore, an in-principle antisymmetric contribution would be negligible, and to make a simplified description to capture the experimental observation, we ignore such virtually negligible complex exchanges in the present case. Moreover the calculated exchange interactions using a symmetric-type exchange in the presence of SOC are able to reproduce the experimental trend transition temperatures in this series of compounds. Calculated magnetocrystalline energies (∼1–1.5 meV/f.u.) favor in-plane spin alignment consistent with the experimental observations. A point to be noted for all three compounds is that Os exhibits a rather large orbital moment ($-0.11\mu_B$), oppositely aligned to that of the spin moments, which is expected for less than half-filled configurations. Although for the half-filled t_{2g} case, orbital moments should be quenched, and large orbital moments may arise from strong mixing with O-2p states as mentioned in the literature [32].

From our calculations we found that SOC is really important to understand the magnetism in these Os-based double perovskites. We found a significant orbital moment at the Os site, which is counterintuitive considering the half-filled t_{2g} orbitals. The effective moment is substantially smaller than what would be expected from a spin-only value for the $S = 3/2$ ($3.89\mu_B$) state and that only can be explained by taking both the positive spin moment and the negative orbital moment into account. Therefore, our results go with the results presented in Ref. [31] in the context of Ba_2YOsO_6, the results shown in Refs. [33,34] in the context of Sr_2CrOsO_6, and contrary to the result presented in Ref. [35] in the context of Sr_2CrOsO_6. In Ref. [35], the authors did not find any evidence of an orbital moment at the Os site, and based on that, they claimed that SOC is not responsible for the finite net moment. Moreover, in the present series, we found that the experimentally observed AFM structure can only be stabilized with the inclusion of SOC. Therefore, our results suggest that SOC is important

for understanding the magnetic behaviors in these materials, however, only the symmetric type of exchange is enough to understand the basic experimental observations.

Because $Os^{5+}(5d^3)$ is the only magnetically active site in the two isostructural, isoelectronic, and isovalent compounds, a common expectation is that they should show similar magnetic interactions. Moreover, it is generally believed that nonmagnetic cations do not play any active role in determining magnetic interactions and transition temperatures. Our studies show an opposite scenario. For SYOO and SIOO, Os^{5+} has a $5d^3$ configuration, whereas Y^{3+} and In^{3+} have $4d^0$ and $4d^{10}$ valence configurations, respectively. The superexchange interactions between the two Os sites are mediated by nonmagnetic oxygen and Y or In states. Because Y^{3+} has an open $4d$ shell, it is strongly hybridized with the empty Os-e_g states as revealed by large Os-d tails at the Y sites in the Wannier plots (marked by circles) and the energy overlap in the DOS. This allows for the hopping of Os electrons via empty Y-$4d$ orbitals. In the case of In^{3+}, the closed-shell d^{10} configuration, which is deep in the energy scale, does not allow the Os electrons to hop. To generalize this mechanism of hybridization-driven enhancement of magnetic interactions beyond the present two $4d$-$5d$ compounds, we cross-checked our scheme with the $3d$-$5d$ system in SSOO. The calculated magnetic exchange interactions of SSOO are much stronger than that of SYOO. The largest exchange interaction in SSOO is largest among these three compounds and is readily explained by the very strong hybridization between empty Os-e_g states and Sc-$3d$ states, which overlap over almost the entire energy range as shown in the bottom panel of Fig. 1. To compare these findings with the experimental results, we calculated the mean-field transition temperatures for SSOO, SYOO, and SIOO using the calculated magnetic exchange interactions. We found that the calculated ratio of mean-field transition temperature $T_N^{YOs}/T_N^{InOs} \sim 2.64$ (GGA), 2.90 (GGA + U), 2.51 (GGA + SOC), and $T_N^{ScOs}/T_N^{YOs} \sim 1.64$ (GGA), 1.66 (GGA + U), and 1.51 (GGA + SOC) agreed reasonably well with the experimental T_N ratios of 2.04 and 1.73, respectively. This analysis shows that, even though Y, In, and Sc are nonmagnetic, their electronic configurations, either open shell or closed shell, will increase or decrease hybridization with the Os states which dictate the strength of the overall magnetic exchange interactions and affects the magnetic transition temperatures of the materials.

A relevant question is whether the observed trend in exchange interactions is due to differences of orbital hybridization induced by the volume contraction and structural distortion of each compound. It is evident from Table I, although exact values of the bond lengths and angles differ among the three compounds, that there are no drastic structural changes. To clarify this point we calculated the exchange interactions of the three compounds within the unit-cell volumes of the other compounds. The results are summarized in Table III. We found that the trend in exchange interactions remains unchanged with maximum differences of absolute values of only $\pm 20\%$, which confirms that electronic-configuration-induced hybridization not volume is the principal determining factor.

Conclusion. To summarize, we did a comparative analysis of magnetic interactions in the double perovskites, SYOO, SIOO, and SSOO with a single magnetically active Os site using DFT-based first-principles calculations. Although it is known that nonmagnetic cations may influence magnetic interactions, our studies provide direct evidence of the role played by the electronic configurations of nonmagnetic transition-metal cations. Our calculations reveal short-range Os-Os interactions are stronger than long-range Os-Os interactions in the present compounds unlike previous $3d$-$5d$ compounds (Sr_2FeOsO_6 and Sr_2CoOsO_6). Although Y^{3+}/Sc^{3+} and In^{3+} are nonmagnetic, their electronic configurations, i.e., open shell (d^0) or closed shell (d^{10}), strongly influence hybridization with the Os states and the strength of exchange coupling. This leads to the largest T_N for SSOO and the smallest for SIOO, which is consistent with both calculation and experimental observations. The hybridization-driven mechanism of enhanced magnetic coupling successfully explains the observed trend in T_N for these systems investigated and can be generalized to the other systems. Our investigation also revealed the importance of SOC in terms of symmetric exchange to understand the magnetism in this series of materials. Our studies highlight the importance of understanding single active site d^3 materials and open up a direction for further research in the control of T_N for double perovskites with single and double magnetic sites.

[1] K. I. Kobayashi, T. Kimura, H. Sawada, K. Terakura, and Y. Tokura, Nature (London) **395**, 677 (1998).

[2] M. Azuma, K. Takata, T. Saito, S. Ishiwata, Y. Shimakawa, and M. Takano, J. Am. Chem. Soc. **127**, 8889 (2005).

[3] N. S. Rogado, J. Li, A. W. Sleight, and M. A. Subramanian, Adv. Mater. **17**, 2225 (2005).

[4] H. Das, M. De Roychaudhury, and T. Saha-Dasgupta, Appl. Phys. Lett. **92**, 201912 (2008).

[5] Y. Krockenberger, K. Mogare, M. Reehuis, M. Tovar, M. Jansen, G. Vaitheeswaran, V. Kanchana, F. Bultmark, A. Delin, F. Wilhelm, A. Rogalev, A. Winkler, and L. Alff, Phys. Rev. B **75**, 020404 (2007).

[6] M. Retuerto, J. A. Alonso, M. García-Hernández, and M. J. Martínez-Lope, Solid State Commun. **139**, 19 (2006).

[7] J. B. Philipp, P. Majewski, L. Alff, A. Erb, R. Gross, T. Graf, M. S. Brandt, J. Simon, T. Walther, W. Mader, D. Topwal, and D. D. Sarma, Phys. Rev. B **68**, 144431 (2003).

[8] H. Kato, T. Okuda, Y. Okimoto, Y. Tomioka, Y. Takenoya, A. Ohkubo, M. Kawasaki, and Y. Tokura, Appl. Phys. Lett. **81**, 328 (2002).

[9] B. Yan, A. K. Paul, S. Kanungo, M. Reehuis, A. Hoser, D. M. Többens, W. Schnelle, R. C. Williams, T. Lancaster, F. Xiao, J. S. Möller, S. J. Blundell, W. Hayes, C. Felser, and M. Jansen, Phys. Rev. Lett. **112**, 147202 (2014).

[10] R. Morrow, R. Mishra, O. D. Restrepo, M. R. Ball, W. Windl, S. Wurmehl, U. Stockert, B. Buchner, and P. M. Woodward, J. Am. Chem. Soc. **135**, 18824 (2013).

[11] S. Kanungo, B. Yan, M. Jansen, and C. Felser, Phys. Rev. B **89**, 214414 (2014).

[12] A. K Paul, M. Reehuis, V. Ksenofontov, B. Yan, A. Hoser, D. M. Többens, P. M. Abdala, P. Adler, M. Jansen, and C. Felser, Phys. Rev. Lett. **111**, 167205 (2013).

[13] A. K. Paul, A. Sarapulova, P. Adler, M. Reehuis, S. Kanungo, D. Mikhailova, W. Schnelle, Z. Hu, C. Kuo, V. Siruguri, S. Rayaprol, Y. Soo, B. Yan, C. Felser, L. H. Tjeng, and M. Jansen, Z. Anorg. Allg. Chem. **641**, 197 (2015).

[14] A. E. Taylor, R. Morrow, D. J. Singh, S. Calder, M. D. Lumsden, P. M. Woodward, and A. D. Christianson, Phys. Rev. B **91**, 100406 (2015).

[15] D. Reinen, M. Atanasov, and S.-L. Lee, Coord. Chem. Rev. **175**, 91 (1998).

[16] D. Reinen, Theor. Chim. Acta **5**, 312 (1966).

[17] G. Kresse and J. Hafner, Phys. Rev. B **47**, 558(R) (1993); G. Kresse and J. Furthmüller, *ibid.* **54**, 11169 (1996).

[18] J. P. Perdew, K. Burke, and M. Ernzerhof, Phys. Rev. Lett. **77**, 3865 (1996).

[19] V. I. Anisimov, J. Zaanen, and O. K. Andersen, Phys. Rev. B **44**, 943 (1991); V. I. Anisimov, A. I. Poteryaev, M. A. Korotin, A. O. Anokhin, and G. Kotliar, J. Phys.: Condens. Matter **9**, 7359 (1997).

[20] S. L. Dudarev, G. A. Botton, S. Y. Savrasov, C. J. Humphreys, and A. P. Sutton, Phys. Rev. B **57**, 1505 (1998).

[21] K. Samanta, P. Sanyal, and T. Saha-Dasgupta, Sci. Rep. **5**, 15010 (2015).

[22] See Supplemental Material at http://link.aps.org/supplemental/10.1103/PhysRevB.93.161116 for a systematic analysis of the electronic structure.

[23] K. I. Kugel, and D. I. Khomskii, Sov. Phys. JETP **37**, 725 (1973); Sov. Phys. Usp. **25**, 231 (1982).

[24] V. V. Mazurenko, F. Mila, and V. I. Anisimov, Phys. Rev. B **73**, 014418 (2006).

[25] C. S. Helberg, W. E. Pickett, L. I. Boyer, H. T. Stokes, and M. J. Mehl, J. Phys. Soc. Jpn. **68**, 3489 (1999).

[26] S. Sarkar, S. Kanungo, and T. Saha-Dasgupta, Phys. Rev. B **82**, 235122 (2010).

[27] M. Majumder, S. Kanungo, A. Ghoshray, M. Ghosh, and K. Ghoshray, Phys. Rev. B **91**, 104422 (2015).

[28] X. Ou, Z. Li, F. Fan, H. Wang, and H. Wu, Sci. Rep. **4**, 7542 (2014).

[29] H. Matsuura and K. Miyake, J. Phys. Soc. Jpn. **82**, 073703 (2013).

[30] A. A. Aczel, D. E. Bugaris, L. Li, J.-Q. Yan, C. de la Cruz, H.-C. zur Loye, and S. E. Nagler, Phys. Rev. B **87**, 014435 (2013); A. A. Aczel, P. J. Baker, D. E. Bugaris, J. Yeon, H.-C. zur Loye, T. Guidi, and D. T. Adroja, Phys. Rev. Lett. **112**, 117603 (2014).

[31] E. Kermarrec, C. A. Marjerrison, C. M. Thompson, D. D. Maharaj, K. Levin, S. Kroeker, G. E. Granroth, R. Flacau, Z. Yamani, J. E. Greedan, and B. D. Gaulin, Phys. Rev. B **91**, 075133 (2015).

[32] C. Jia, S. Onoda, N. Nagaosa, and J. H. Han, Phys. Rev. B **76**, 144424 (2007).

[33] H. Das, P. Sanyal, T. Saha-Dasgupta, and D. D. Sarma, Phys. Rev. B **83**, 104418 (2011).

[34] K.-W. Lee and W. E. Pickett, Phys. Rev. B **77**, 115101 (2008).

[35] O. N. Meetei, O. Erten, M. Randeria, N. Trivedi, and P. Woodward, Phys. Rev. Lett. **110**, 087203 (2013).